JOURNAL OF Materials CHEMISTRY

Synthesis and characterization of europium-doped ordered mesoporous silicas

Jivaldo R. Matos,[a]† Lucildes P. Mercuri,[a]† Mietek Jaroniec,*[a] Michal Kruk,[a] Yasuhiro Sakamoto[b] and Osamu Terasaki[b,c]

[a]*Department of Chemistry, Kent State University, Kent, Ohio, 44240, USA. E-mail: Jaroniec@columbo.kent.edu*
[b]*Department of Physics, Graduate School of Science and Center of Interdisciplinary Research, Tohoku University, Sendai 980-77, Japan*
[c]*CREST, Japan Science and Technology Corporation, Japan*

Received 6th March 2001, Accepted 22nd June 2001
First published as an Advance Article on the web 7th August 2000

Silica mesoporous molecular sieves doped with europium were synthesized using Cab-O-Sil M5 silica and europium chloride in the presence of cetyltrimethylammonium bromide surfactant. The materials obtained with lower Eu content (Si : Eu molar ratio of 100) in the synthesis gel exhibited two-dimensional hexagonally ordered structure of the MCM-41 type, whereas larger Eu contents resulted in lower size of hexagonally ordered porous domains (for Si : Eu = 33) or in disordered porous structures (for Si : Eu = 20). The pore size increased from 3.4 to 4.0 nm as the amount of Eu in the synthesis mixture increased. Pore size distributions (PSDs) for Eu-doped silicas were narrower than the PSDs of the pure-silica MCM-41 material synthesized under the same conditions. A decrease in the specific surface area and primary mesopore volume was observed for higher Eu loadings. The volume of secondary (interparticle) pores increased as the content of Eu in the synthesis gel increased, which is consistent with the transmission electron microscopy images that provided an indication of the decrease in the particle size, although the latter was not uniform throughout the materials under study. Energy dispersive X-ray fluorescence (EDX) data indicated that europium is indeed present in the structure of the materials studied, although its content tended to be somewhat lower than that in the synthesis gel and its distribution within the materials appeared to be non-uniform. The synthesis procedure reported herein was used to synthesize silicas doped with other lanthanides, and for given lanthanide loadings, the resultant materials exhibited porous structures similar to those of the Eu-doped samples.

Introduction

The synthesis of mesoporous molecular sieve silicas with framework-incorporated or grafted heteroatoms has received much attention during the last decade. Initially, aluminium-,[1] titanium-,[2,3] and vanadium-incorporated[4] MCM-41 and HMS silicas were reported, which was followed by a large number of studies on the incorporation or surface grafting of these and other metals.[5,6] The resulting materials were found to be useful as acid and redox catalysts.[5,6] The possibility of doping ordered mesoporous silicas with lanthanides attracted relatively little attention (here lanthanum is considered as a lanthanide). This is somewhat surprising because the beneficial effects of lanthanide or lanthanide oxide doping of porous silicas and aluminas are well known. For instance, cerium oxide is used as an additive for preparation of automobile converter catalysts to enhance performance and stability.[7,8] Lanthanum and cerium have been used as promoters of noble metal catalysts.[9,10] The effect of the promotion was observed despite the lack of catalytic activity for pure lanthanide oxides. Other applications of lanthanide-doped materials include photocatalysis, optical amplifiers, micro lasers, and luminescent labels (see ref. 11 and references therein). Despite all these beneficial features of lanthanides, their incorporation or grafting on the surfaces of ordered mesoporous materials was discussed only in a few studies.[12–23] In particular, the synthesis of La-doped MCM-41 was reported, wherein the evidence was found for incorporation of these heteroatoms in the framework of as-synthesized materials, whereas calcined samples were suggested to contain mostly extra-framework lanthanide oxides.[12–15] Doping of the aluminosilicate MCM-41 with lanthanum resulted in a moderate improvement of its thermal stability.[16] The synthesis of Ce-doped (as well as La-doped) MCM-41 was also accomplished.[17–19] Ce- and La-doped aluminas with wormlike pores exhibited improved porous structures and enhanced thermal stability.[20] Impregnation of MCM-41 with caesium acetete and lanthanum nitrite allowed for the synthesis of a stable basic catalyst with an active $CsLaO_x$ phase.[21] Moreover, neodymium silylamide precursors have been grafted on the surface of siliceous MCM-41.[22,23] Herein, we report the synthesis and characterization of europium-doped ordered mesoporous silicas. The synthesis procedure employed in this study can be used to obtain silicas doped with other lanthanides, and the structures of the resultant materials are similar to those reported herein for the corresponding lanthanide doping level.

Experimental

Synthesis

The pure-silica and europium-doped samples were synthesized *via* a hydrothermal method similar to that reported in ref. 24. Cab-O-Sil M-5 silica (Cabot Co.), Eu_2O_3 (Sigma), hydrochloric

†Permanent address: Instituto de Química da Universidade de São Paulo, C.P. 26.077, 05599-970, São Paulo, SP, Brazil.

 DOI: 10.1039/b102056k

acid (Fisher Scientific), cetyltrimethylammonium bromide (CTMABr) (Aldrich) and 97% tetramethylammonium hydroxide pentahydrate (TMAOH·5H_2O) (Fisher Scientific) were used as received. The synthesis mixture had the following molar composition: 1.0 SiO_2 : 0.317 TMAOH : 0.45 CTMABr : x Eu_2O_3 : 18x HCl : 67 H_2O (x = 0.000, 0.005, 0.015 and 0.025). In a typical synthesis for x = 0.015, TMAOH·5H_2O (1.48 g) was dissolved in 20.0 g of water and 4.09 g of CTMABr was added to the TMAOH solution under vigorous mechanical stirring (the pH of the mixture was equal to 13.5). Then, 0.132 g of Eu_2O_3 was dissolved in 3.5 g of 2 M HCl solution under heating at about 343 K, and after cooling, the resultant solution was added to the TMAOH–CTMABr mixture. The remaining amount of water was added to the synthesis mixture to reach a mass of 30.1 g (the pH of the mixture was 12.8). After 15 min of stirring, 1.5 g of Cab-O-sil silica was added and the stirring was continued for the next 30 min, after which pH dropped to 12.5. The resulting gel was transferred into a Teflon-lined autoclave, and heated statically under autogenous pressure for 40 h at 373 K. After cooling to room temperature, the pH of the mixture was 12.2. The resulting solid product was filtered off and washed extensively with deionized water and dried at room temperature. The samples were calcined under flowing nitrogen and subsequently air (100 mL min^{-1} flow). The temperature was increased from ambient to 813 K using a heating rate of 1 K min^{-1}. After heating for 5 h at 813 K, the flowing gas was switched from nitrogen to air and the heating was continued for an additional 2 h. Selected samples were additionally calcined at higher temperatures. More specifically, one sample calcined at 813 K was subjected to calcination at 973 K for 4 h under air atmosphere with an initial temperature ramp of 2 K min^{-1}. The resulting material was used for nitrogen adsorption measurement and the calcination at 1073 K was performed in the same manner. After the adsorption study, the resulting material was calcined once again at 1173 K. The samples are denoted as follows. The pure-silica material is denoted MS (mesoporous silica), whereas the europium-doped materials are denoted MS-EuX, where X denotes the Si : Eu molar ratio in the synthesis gel (X = 100 for x = 0.005; X = 33 for x = 0.015; X = 20 for x = 0.025). In addition, in the case where two samples synthesized under the same conditions are described, the second is denoted as MS-EuXA. For the samples calcined at temperatures different from 813 K, the calcination temperature is indicated in parentheses. For instance, MS(1173) denotes the pure-silica material calcined at 1173 K.

Characterization

Nitrogen adsorption measurements were carried out using a Micromeritics ASAP 2010 volumetric adsorption analyzer. Before the measurements, the samples were degassed at 473 K in the outgassing port of the adsorption instrument. Weight change curves were recorded under flowing nitrogen on a TA Instruments TGA 2950 high-resolution thermogravimetric analyzer in high-resolution mode with maximum heating rate of 5 K min^{-1}. Powder X-ray diffraction patterns were recorded on a Siemens D5005 diffractometer using Cu-Kα radiation. The FTIR spectra were recorded on a Nicolet Magna 550 spectrometer at 4 cm^{-1} resolution using KBr pellet techniques. A typical pellet contains about 1 wt% sample diluted in KBr (Merck, 99.9%). Transmission electron microscopy (TEM) images were obtained using a JEOL 3010 TEM instrument (accelerating voltage of 300 kV, C_s = 0.6 nm) and recorded on films. Energy dispersive X-ray fluorescence (EDX) measurements were carried out using an Oxford LINK, ISIS 300 spectrometer.

Specific surface areas were calculated using the Brunauer–Emmett–Teller (BET) method.[25] The relative pressure range from 0.04 to 0.08 was used in the BET calculations in order to consistently use the same pressure interval for all samples and to exclude the data from the capillary condensation region. Total pore volumes[25] (*i.e.* the volume of pores narrow enough to exhibit capillary condensation at relative pressures distinguishable from the bulk saturation pressure, which is expected to correspond to the upper pore size limit of about 200–400 nm in the case of nitrogen adsorption at 77 K) were evaluated from the amount of N_2 adsorbed at a relative pressure of about 0.99. The primary mesopore volumes and the external surface areas were evaluated using an α_s plot[25,26] method in an α_s interval from 1.25 to 1.6 (α_s is defined as a ratio of the amount adsorbed for a reference adsorbent at a given relative pressure to the amount adsorbed for this adsorbent at a relative pressure of 0.4). It should be noted that pores are classified herein as micropores (diameter below 2 nm), mesopores (diameter from 2 to 50 nm) and macropores (diameter above 50 nm).[25] Moreover, the uniform mesopores within the particles of the samples under study are referred to as primary mesopores, whereas other mesopores and macropores of the size below *ca.* 200–400 nm are referred to as secondary pores. For the samples under study, the secondary pores can be considered as interparticle pores. The presence of microporosity in the samples was examined using the α_s plot method in an α_s range from 0.0 to 0.6. The pore size distribution (PSD) was calculated using the Barrett–Joyner–Halenda (BJH) algorithm[27] (but without the simplifying assumptions proposed by these authors) and the (pore diameter)–(capillary condensation relative pressure) relation determined recently for a significant range of mesopore sizes using a series of MCM-41 silicas as model adsorbents.[28] The statistical film thickness curve (t-curve) employed in the BJH calculations was also derived using large-pore MCM-41 silicas and extrapolated using the data for a macroporous silica.[28] The t-curve data are reported elsewhere.[26] The pore diameter is defined as the position of the maximum of the PSD.

Results and discussion

Powder X-ray diffraction patterns for calcined pure-silica (MS) and europium-doped materials (MS-Eu100, -Eu33, and -Eu20) are shown in Fig. 1. The pure-silica sample (MS) and the sample with low europium content in the synthesis gel (MS-Eu100) exhibited XRD patterns with three peaks characteristic of the MCM-41 structure[1] that is known to consist of two-dimensional hexagonal (honeycomb) arrays of uniform non-intersecting channel-like pores.[29] The samples synthesized using higher europium contents in the synthesis gel exhibited XRD patterns similar to those of HMS silicas[3] that exhibit disordered interconnected structures with uniform pore diameters.[30,31] It is known that such XRD patterns can also result from the small size of coherently scattering domains of 2-D hexagonally ordered structures.[32,33] Transmission electron

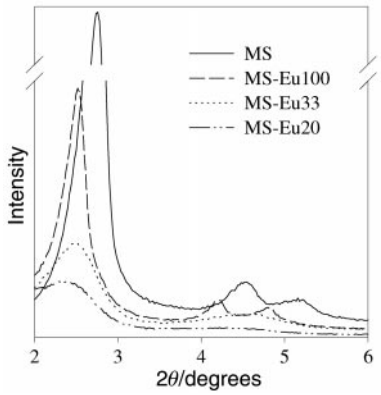

Fig. 1 Powder X-ray diffraction patterns for the pure-silica and europium-doped samples.

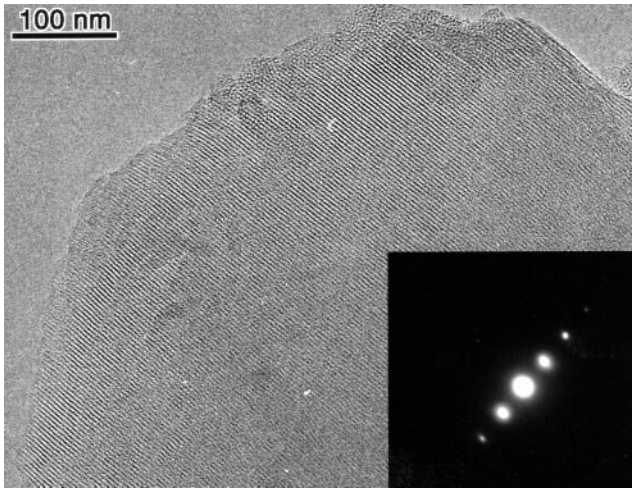

Fig. 2 Transmission electron microscopy image for a particle of the MS-Eu100 sample.

microscopy (TEM) images of the europium-doped materials allowed us to refine this structural identification. Fig. 2 shows an image of a particle of the MS-Eu100 sample taken with [10] incidence. The fringe spacing is about 3.7 nm and corresponds to the [10] lattice fringe of two-dimensional MCM-41 type. This image can be regarded as a side view of a regular arrangement of long nonintersecting channels characteristic of the MCM-41 structure.[34] The particle shown in Fig. 2 was quite large, although TEM imaging also revealed a small amount of much smaller particles with porous systems that appeared to be partially disordered (image not shown). Fig. 3 shows a TEM image of MS-Eu33. In this case, rather small sizes of uniform domains of a 2-D hexagonal phase were observed (as seen from the appearance of regions showing honeycomb structures, as well as side views of honeycomb structures, *i.e.* parallel lines with uniform spacing) along with some domains that appear to have disordered porosity.[32] These apparently disordered domains in MS-Eu100 and -Eu33 structures may actually be hexagonally ordered ones imaged with the incident electron beam that is neither parallel nor perpendicular to the ordered channels. As will be shown later, the primary mesoporosity of MS-Eu100 and -Eu33 was of uniform size, which makes the presence of two different types of pore structure arrangements somewhat unlikely. The porous

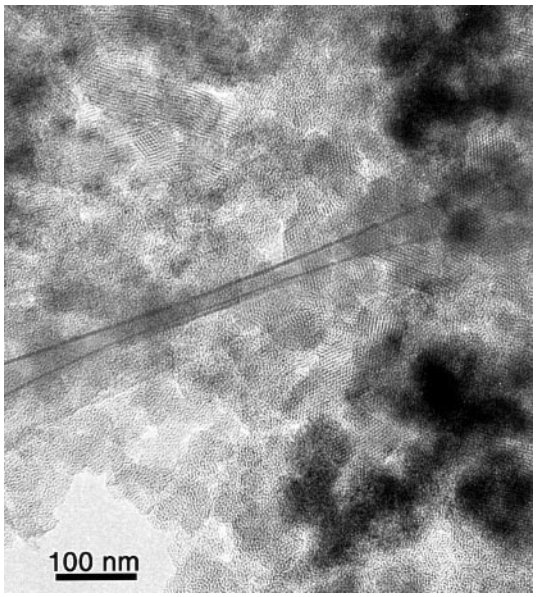

Fig. 3 Transmission electron microscopy image of the MS-Eu33 sample.

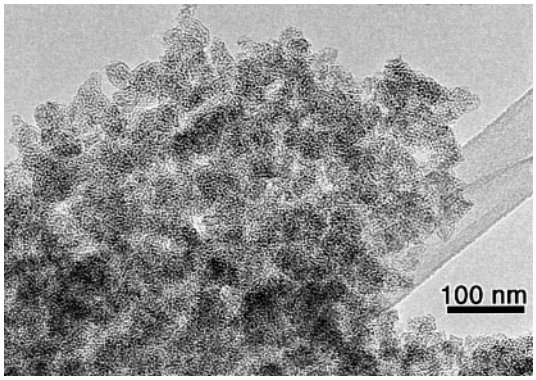

Fig. 4 Transmission electron microscopy image of the MS-Eu20 sample.

domains appear to be randomly oriented within aggregates in such a way that some porosity between domains was observed. The TEM image of MS-Eu20 (Fig. 4) indicated a disordered structure of primary pores in the material. These pores appear to be located in particles of size well below 100 nm, and these particles themselves were agglomerated into much larger structures with appreciable interparticular pores.

It is known that doping of heteroatoms during the synthesis of ordered mesoporous silicas might produce different effects in terms of the degree of incorporation of heteroatoms in the resultant materials. Some heteroatoms can be incorporated into the silica framework when synthesis conditions are appropriate.[5,6] Other heteroatoms may be more difficult to incorporate and may have a tendency to form extra-framework species,[5,6] or their content in the resultant materials may be much lower than that in the synthesis gel.[35] As inferred from EDX analysis, europium was indeed incorporated in the samples, although the molar percentages appeared to be somewhat lower than those in the synthesis gel. For the samples with the molar Si : Eu ratios in the synthesis gel of 100 : 1 (MS-Eu100), 33 : 1 (Eu33) and 20 : 1 (MS–Eu20), average molar Si : Eu ratios in the calcined samples estimated from the EDX data were about 186 : 1, 34 : 1, and 26 : 1, respectively. However, the data for particular samples exhibited significant variations, thus indicating that the distribution of europium in the samples may be quite inhomogeneous. FTIR spectra provided an additional insight into the problem of the europium location in the structure of the samples under study. The FTIR spectra were generally similar to those of amorphous silicas (compare Fig. 5 with the data reported in ref. 36). However, positions of bands corresponding to asymmetric stretching and bending modes of internal tetrahedral vibrations in the silica-based structure[37] were shifted to higher frequencies. More specifically, the asymmetric stretch band shifted from 1059 cm^{-1} for as-synthesized MS silica, to 1065, 1068 and 1074 cm^{-1} for MS-Eu100, -Eu33, and -Eu20, respectively. The corresponding shift for the calcined materials was from 1086 to 1088, 1089 and 1092 cm^{-1}, respectively. Likewise, the bending mode band shifted from 455 cm^{-1} for as-synthesized MS silica, to 456, 457 and 461 cm^{-1} for MS-Eu100, -Eu33, and -Eu20, respectively, and the corresponding shift for the calcined materials was from 461 to 465, 467 and 469 cm^{-1}, respectively. A similar shift to higher wavenumbers has been reported for zeolites with sodium ions exchanged for lanthanide ions[38] and for La- and Ce-doped MCM-41,[17] but a shift to lower wavenumbers was observed in other studies of La-doped MCM-41.[12,15] Nonetheless, it is clear that the presence of europium affects the silica framework vibrations for the samples under current study, thus indicating some degree of incorporation of europium in the framework, or the presence of extra-framework europium species in close contact with the framework. The latter would suggest that if

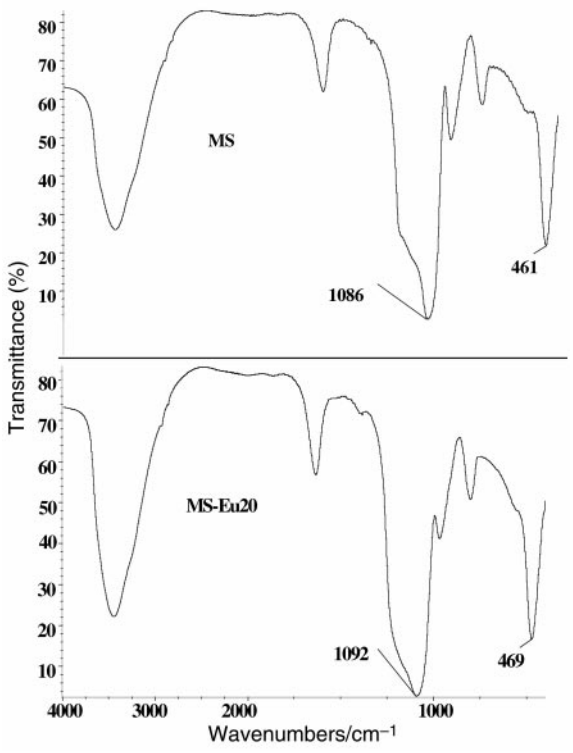

Fig. 5 FTIR spectra for selected samples under study.

extra-framework europium species were present, they were highly dispersed on the silica surface. It can be expected from previous studies of cerium- and lanthanium-doped MCM-41 silica that lanthanides are likely to be incorporated to some extent in the silicate framework of as-synthesized MCM-41. However, they are not retained in the framework after the calcination and form extra-framework lanthanide oxides. Similar behavior is likely for the samples under current study, although verification of this will require further studies.

Thermogravimetric analysis indicated that the contents of surfactant (approximated by the weight loss from about 373 to 623 K) in as-synthesized materials were very similar for the pure-silica sample and the MS-Eu100 samples with lowest europium content (see Fig. 6). However, the as-synthesized materials with higher europium contents (MS-Eu33A and MS-Eu20) exhibited a tendency to contain a gradually reduced surfactant content. The as-synthesized MS-Eu33 sample was exceptional, because it exhibited an unexpectedly large weight loss in the surfactant decomposition temperature range, perhaps because of the retention of some excess (non-templating) surfactant after washing. For the europium-doped materials,

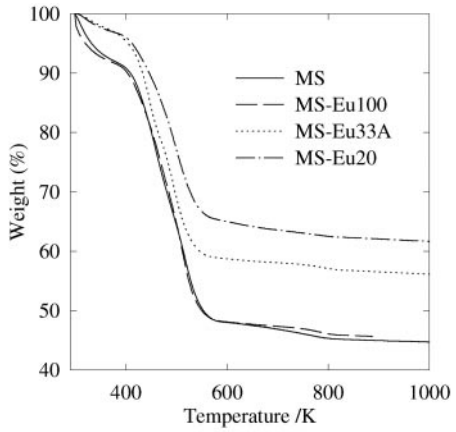

Fig. 6 Weight change curves for as-synthesized pure-silica and europium-doped samples.

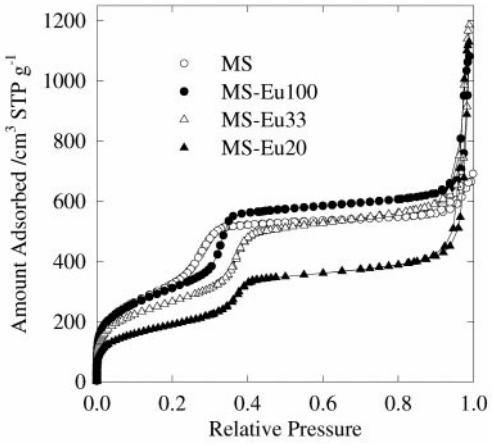

Fig. 7 Nitrogen adsorption isotherms for the pure-silica and europium-doped samples.

no correlation between the weight loss between about 573 and 723 K and the heteroatom content was observed, in contrast to the behavior observed for some other heteroatoms, such as aluminium.[39]

Nitrogen adsorption isotherms for all the samples under study were generally of the type commonly observed for ordered mesoporous materials[40,41] (see Fig. 7). The adsorption process took place *via* (i) monolayer–multilayer adsorption at lower relative pressures, followed by (ii) capillary condensation in primary mesopores at relative pressures somewhere between 0.25 and 0.45, and subsequently (iii) multilayer buildup on the external surface of particles, and finally (iv) capillary condensation in secondary (interparticle) pores. The step of capillary condensation in primary mesopores shifted to higher relative pressures as the content of europium in the synthesis gel increased. The adsorption capacity of primary mesopores increased for lower europium doping levels and decreased for higher heteroatom loadings. An increase in the heteroatom doping level led also to an increase in the amount adsorbed at relative pressures close to 1, indicating an increase in the volume of interparticle pores of size below about 200 nm.

Structural information about the samples derived from nitrogen adsorption data is listed in Table 1. It can be seen that the BET specific surface area was similar for the pure-silica and the MS-Eu100 samples, but further increase in the heteroatom doping level led to a decrease in the specific surface area. The pore diameter increased and the width of PSD was reduced as the content of heteroatoms increased (see Fig. 8). An improved uniformity of the pore size in the materials with larger europium content (MS-Eu33 and -Eu20) appears to contradict the XRD data that showed an increase in the structural

Table 1 Structural properties of pure and europium-doped ordered mesoporous silicas

Sample	S_{BET}/ $m^2\ g^{-1}$	V_t/ $cm^3\ g^{-1}$	V_p/ $cm^3\ g^{-1}$	S_{ex}/ $m^2\ g^{-1}$	w/ nm
MS	1120	1.03	0.77	90	3.4
MS(973)	1030	0.88	0.66	80	3.2
MS(1073)	960	0.82	0.59	80	3.0
MS(1173)	850	0.63	0.44	60	2.6
MS-Eu100	1090	1.67	0.79	170	3.7
MS-Eu100A	1140	1.22	0.80	130	3.6
MS-Eu100A(973)	1100	1.14	0.76	120	3.5
MS-Eu100A(1073)	1020	1.00	0.68	110	3.3
MS-Eu100A(1173)	910	0.84	0.55	80	3.0
MS-Eu33	940	1.83	0.65	260	3.9
MS-Eu33A	920	2.06	0.57	300	3.9
MS-Eu20	670	1.75	0.42	220	4.0

[a] S_{BET}, BET specific surface area; V_t, total pore volume; V_p, primary mesopore volume; S_{ex}, external surface area; w, pore diameter.

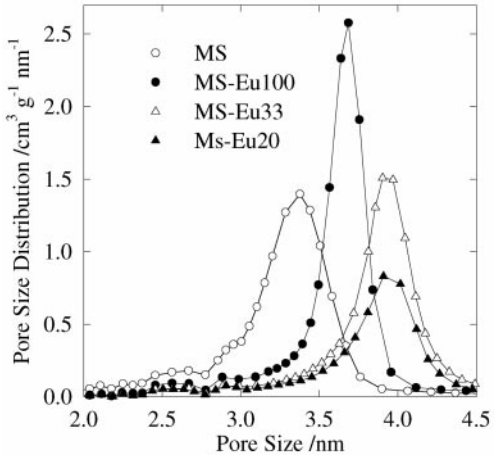

Fig. 8 Pore size distributions for the pure-silica and europium-doped samples.

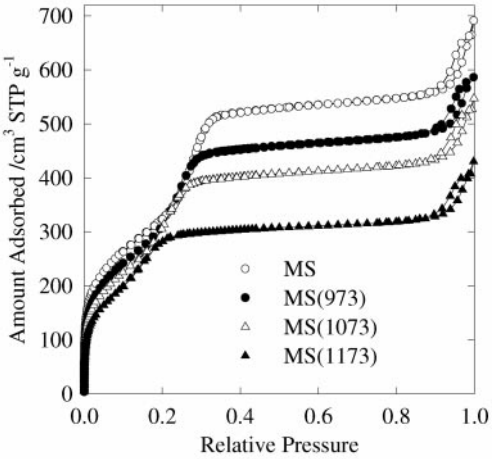

Fig. 9 Nitrogen adsorption isotherms for the pure-silica sample calcined at different temperatures.

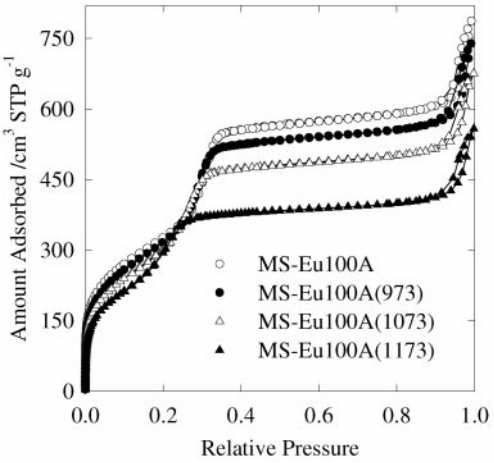

Fig. 10 Nitrogen adsorption isotherms for the europium-doped sample MS-Eu100 calcined at different temperatures.

disordering. However, these results can be reconciled when one takes into consideration that a poor resolution of the XRD patterns may result not only from poor structural ordering but also from small size of coherently scattering domains. As discussed above and will also be confirmed on the basis of adsorption data, the particle size for the samples doped with Eu appears to decrease as the doping level increases. No microporosity was detected for the samples under study using α_s plot analysis. However, the introduction of europium to the synthesis gel resulted in a slight increase in the low-pressure nitrogen adsorption in comparison to the pure-silica material, as seen from relative adsorption curves (the relative adsorption is defined as the amount adsorbed divided by the BET monolayer capacity). The primary mesopore volume increased, and then decreased as the europium content in the synthesis gel increased, which was accompanied by a fairly systematic increase in the ratio S_{ex}/S_{BET} and secondary (textural) pore volume (difference between the total pore volume and primary mesopore volume). It should be emphasized that the textural pore volume for the samples doped with europium may be comparable or even several times larger (in the case of MS-Eu33B and MS-Eu20) than the primary mesopore volume. This feature was observed in the case of HMS silicas[32] and was shown to lead to improved catalytic activity of heteroatom-incorporated silicas, which was attributed to the improved diffusion properties of the uniform porous structure with appreciable textural porosity.[42] Therefore, the significant textural porosity of the europium-doped mesoporous silicas studied herein may be beneficial in applications requiring good transport properties of the overall porous structure. It should be noted that the synthesis procedure reported herein was found to be highly reproducible as far as the specific surface area, primary mesopore diameter, and primary mesopore volume is concerned (see data for MS-Eu100 and MS-Eu100A, as well as MS-Eu33 and MS-Eu33A listed in Table 1). The secondary pore volume was less reproducible, but it also should be noted that the determination of this quantity is quite inaccurate for the samples whose adsorption isotherms exhibit an abrupt increase close to the saturation vapor pressure, as was the case for the europium-doped materials.

To further compare the properties of pure-silica and europium-doped materials, their thermal stability was assessed. The MS and MS-Eu100 samples were calcined at 973, 1073 and 1173 K and their nitrogen adsorption isotherms were measured (see Figs. 9 and 10). It can be seen that a decrease in the primary mesopore volume after the high-temperature calcination was larger for the pure-silica material (for instance, 43% for MS *vs.* 31% for MS-Eu100 after calcination at 1173 K). The reduction of the pore diameter and BET specific surface area was also larger for the pure-silica material, which shows that the doping with europium increased the thermal stability of ordered mesoporous silica, similarly to La and Ce doping of porous aluminosilicates[16] and aluminas.[20] When compared to the literature data, the stability of the pure-silica MS sample was moderate, because some MCM-41 samples lost much of their BET specific surface area after calcination below or at 1173 K,[43,44] and other samples were reported to exhibit only a minor surface area loss (about 10%) at these temperatures.[45,46] Even the europium-doped material experienced larger loss of the specific surface area than the aforementioned MCM-41 samples. However, it needs to be kept in mind that in the current study, the relative pressure range used for the BET calculations was chosen in such a way that the data in the capillary condensation region were excluded even for the samples that experience a major decrease in the capillary condensation pressure after the heat treatment. It is not clear if the same precautionary measures were taken in the studies reported in the literature, and thus a possibility of some degree of the BET specific surface area overestimation resulting from the inclusion of data in the capillary condensation range cannot be excluded. This would suggest a higher thermal stability than the actual stability. It also should be noted that among different ordered mesoporous silicas, MCM-41 appears to exhibit only a moderate thermal stability, inferior to FSM-16,[47] and other silicas derived from kanemite,[48] as well as MSU-G,[49] though superior to MCM-48 (as inferred from data reported in ref. 50).

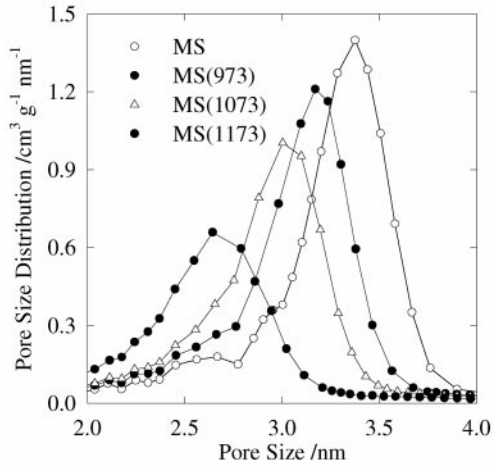

Fig. 11 Pore size distributions for the pure-silica sample calcined at different temperatures.

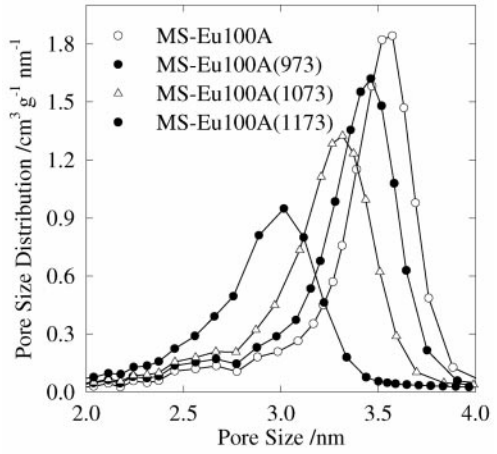

Fig. 12 Pore size distributions for the europium-doped sample MS-Eu100A calcined at different temperatures.

Calcination at 1173 K led to a noticeable broadening of PSD, whereas the treatments at lower temperatures resulted primarily in the shift of PSD toward smaller pore sizes (see Figs. 11 and 12). As the calcination temperature increased, the step corresponding to the capillary condensation in primary mesopores gradually became less pronounced (see Figs. 7 and 8). However, it is known that the capillary condensation step for MCM-41 becomes less distinct for the samples that exhibit capillary condensation at lower relative pressures because of their smaller pore sizes,[51] and even highly ordered samples may exhibit poorly pronounced steps when their pore size is close to the micropore range.[52] Therefore, the broadening and even disappearance of the capillary condensation steps on adsorption isotherms after the high-temperature heat treatment cannot be regarded as convincing evidence of a partial or complete collapse of ordered mesopores, as suggested in some studies,[53,54] although this interpretation may be correct for some samples. This is because the aforementioned changes may merely result from a decrease in the mesopore size, especially if the latter is accompanied with a broadening of the PSD, as for the MS sample studied herein. Furthermore, the shrinkage that accompanies the heat treatment leads to a decrease in the pore volume, so even a dramatic decrease in the pore volume upon high-temperature calcination may not be the result of any appreciable degree of collapse of the ordered domains. It is also interesting to note here that the high temperature calcination resulted in a small, gradual decrease in the relative adsorption at low pressures both for pure-silica (MS) and europium-doped (MS-Eu100) samples, which can be attributed to dehydroxylation, and thus removal of strongly interacting adsorption sites.[55]

In the current study, the results were presented only for europium-doped mesoporous molecular sieve silicas. Similarly structured materials were also synthesized for other lanthanides (lanthanum, cerium, praseodymium, neodymium, samarium, terbium, erbium and ytterbium). The resultant materials with the same contents of different lanthanides in the synthesis gel exhibited very similar pore sizes, BET specific surface areas, pore volumes and secondary porosities as the europium-doped samples. Thus, the synthesis procedure reported herein is not only reproducible for europium-doped silicas, but is general for lanthanide-doped silicas. The properties of mesoporous molecular sieve silicas doped with several different lanthanides will be reported elsewhere.

Conclusions

The addition of europium chloride to a synthesis mixture suitable for MCM-41 preparation resulted in the formation of mesoporous silicas with structural properties dependent on the europium doping level. An increase in the content of europium in the synthesis gel led to an increase in the primary pore size and the volume of secondary pores. The BET specific surface area and the primary pore volume were reduced for higher europium contents. The addition of small or moderate amounts of europium to the synthesis gel resulted in the improvement of uniformity of the primary mesopore size. However, the long-range ordering of the porous structure was diminished for moderate or high europium contents. Both pure-silica and europium-doped samples exhibited good thermal stability, but the doping of europium to the silica framework was clearly beneficial from this point of view. Europium is indeed present in the structure of calcined samples, although its content tends to be smaller than that in the synthesis gel and its distribution within the structure appears to be non-uniform. The location of europium within the structure will require further studies.

Acknowledgements

J. R. M. and L. P. M. are thankful for support from Fundação de Amparo à Pesquisa do Estado de São Paulo (FAPESP), fellowships under grants 99/11170-5 and 99/11171-1. M. J. and M. K. gratefully acknowledge the donors of Petroleum Research Fund administered by the American Chemical Society for support of this research. Dr. S. D. Huang and Mr C. Liu (Kent State University) are acknowledged for XRD measurements. Mr M. S. Filho is gratefully acknowledged for FTIR measurements.

References

1 J. S. Beck, J. C. Vartuli, W. J. Roth, M. E. Leonowicz, C. T. Kresge, K. D. Schmitt, C. T-W. Chu, D. H. Olson, E. W. Sheppard, S. B. McCullen, J. B. Higgins and J. L. Schlenker, *J. Am. Chem. Soc.*, 1992, **114**, 10834.
2 A. Corma, M. T. Navarro and J. Perez Pariente, *J. Chem. Soc., Chem. Commun.*, 1994, 147.
3 P. T. Tanev, M. Chibwe and T. J. Pinnavaia, *Nature*, 1994, **368**, 321.
4 K. M. Reddy, I. Moudrakovski and A. Sayari, *J. Chem. Soc., Chem. Commun.*, 1994, 1059.
5 A. Sayari, *Chem. Mater.*, 1996, **8**, 1840.
6 A. Corma, *Chem. Rev.*, 1997, **97**, 2373.
7 K. R. Krause, P. Schabes-Retchkiman and L. D. Schmidt, *J. Catal.*, 1992, **134**, 204.
8 G. Colon, M. Pijolat, F. Vadivieso, H. Vidal, J. Kaspar, E. Finocchio, M. Daturi, C. Binet, J. C. Lavalley, R. T. Baker and S. Bernal, *J. Chem. Soc., Faraday Trans.*, 1998, **94**, 3717.

9 K. Kili and F. L. Normand, *J. Mol. Catal. A: Chem.*, 1999, **140**, 267.
10 R. Burch and T. C. Watling, *Appl. Catal.*, 1997, **11**, 207.
11 A. Para, E. Sominska, S. Ramesh, Y. Koltypin, Z. Zhong, H. Minti, R. Reisfeld and A. Gedanken, *J. Phys. Chem. B*, 1999, **103**, 3361.
12 N.-Y. He, S.-L. Bao and Q.-H. Xu, *Stud. Surf. Sci. Catal.*, 1997, **105**, 85.
13 N. He, Z. Lu, C. Yuan, J. Hong, C. Yang, S. Bao and Q. Xu, *Supramol. Sci.*, 1998, **5**, 553.
14 N. He, D. Li, M. Tu, J. Shen, S. Bao and Q. Xu, *J. Therm. Anal. Calorimetry*, 1999, **58**, 455.
15 Y. Kuang, N. He, J. Wang, P. Xiao, C. Yuan and Z. Lu, *Colloid Surf. A: Physicochem. Eng. Asp.*, 2001, **179**, 177.
16 L. Y. Chen, S. Jaenicke and G. K. Chuah, *Microporous Mater.*, 1997, **12**, 323.
17 A. S. Araujo and M. Jaroniec, *J. Colloid Interface Sci.*, 1999, **218**, 462.
18 A. S. Araujo and M. Jaroniec, *Stud. Surf. Sci. Catal.*, 2000, **129**, 187.
19 A. S. Araujo and M. Jaroniec, *Thermochim. Acta*, 2000, **345**, 173.
20 W. Zhang and T. J. Pinnavaia, *Chem. Commun.*, 1998, 1185.
21 K. R. Kloetstra, M. van Laren and H. van Bekkum, *J. Chem. Soc., Faraday Trans.*, 1997, **93**, 1211.
22 R. Anwander and R. Roesky, *J. Chem. Soc., Dalton Trans.*, 1997, 137.
23 R. Anwander and C. Palm, *Stud. Surf. Sci. Catal.*, 1998, **117**, 413.
24 A. Sayari and Y. Yang, *J. Phys. Chem. B*, 2000, **104**, 4835.
25 K. S. W. Sing, D. H. Everett, R. A. W. Haul, L. Moscou, R. A. Pierotti, J. Rouquerol and T. Siemieniewska, *Pure Appl. Chem.*, 1985, **57**, 603.
26 M. Jaroniec, M. Kruk and J. P. Olivier, *Langmuir*, 1999, **15**, 5410.
27 E. P. Barrett, L. G. Joyner and P. P. Halenda, *J. Am. Chem. Soc.*, 1951, **73**, 373.
28 M. Kruk, M. Jaroniec and A. Sayari, *Langmuir*, 1997, **13**, 6267.
29 M. Kruk, M. Jaroniec, Y. Sakamoto, O. Terasaki, R. Ryoo and C. H. Ko, *J. Phys. Chem. B*, 2000, **104**, 292.
30 T. J. Pinnavaia and W. Zhang, *Stud. Surf. Sci. Catal.*, 1998, **117**, 23.
31 J. Lee, S. Yoon, S. M. Oh, C.-H. Shin and T. Hyeon, *Adv. Mater.*, 2000, **12**, 359.
32 P. T. Tanev and T. J. Pinnavaia, *Science*, 1995, **267**, 865.
33 S. Schacht, M. Janicke and F. Schuth, *Microporous Mesoporous Mater.*, 1998, **22**, 485.
34 A. Chenite, Y. L. Page and A. Sayari, *Chem. Mater.*, 1995, **7**, 1015.
35 M. S. Morey, A. Davidson and G. D. Stucky, *J. Porous Mater.*, 1998, **5**, 195.
36 C.-Y. Chen, H.-X. Li and M. E. Davis, *Microporous Mater.*, 1993, **2**, 17.
37 E. M. Flanigen, H. Khatami and H. A. Szymanski, *ACS Adv. Chem. Ser.*, 1971, **101**, 201.
38 E. Falabella Sousa-Aguiar, V. L. D. Camorim, F. M. Z. Zotin and R. L. C. Santos, *Microporous Mesoporous Mater.*, 1998, **25**, 25.
39 M. Busio, J. Janchen and J. H. C. van Hooff, *Microporous Mater.*, 1995, **5**, 211.
40 O. Franke, G. Schulz-Ekloff, J. Rathousky, J. Starek and A. Zukal, *J. Chem. Soc., Chem. Commun.*, 1993, 724.
41 P. J. Branton, P. G. Hall, K. S. W. Sing, H. Reichert, F. Schuth and K. K. Unger, *J. Chem. Soc., Faraday Trans.*, 1994, **90**, 2965.
42 T. R. Pauly, Y. Liu, T. J. Pinnavaia, S. J. L. Billinge and T. P. Rieker, *J. Am. Chem. Soc.*, 1999, **121**, 8835.
43 P. T. Tanev and T. J. Pinnavaia, *Chem. Mater.*, 1996, **8**, 2068.
44 S. Namba and A. Mochizuka, *Res. Chem. Intermed.*, 1998, **24**, 561.
45 J. M. Kim, J. H. Kwak, S. Jun and R. Ryoo, *J. Phys. Chem. B*, 1995, **99**, 16742.
46 S. Namba, A. Mochiuka and M. Kito, *Stud. Surf. Sci. Catal.*, 1998, **117**, 257.
47 Y. Inaki, H. Yoshida, K. Kimura, S. Inagaki, Y. Fukushima and T. Hattori, *Phys. Chem. Chem. Phys.*, 2000, **2**, 5293.
48 C.-Y. Chen, S.-Q. Xiao and M. E. Davis, *Microporous Mater.*, 1995, **4**, 1.
49 S. S. Kim, W. Zhang and T. J. Pinnavaia, *Science*, 1998, **282**, 1302.
50 K. Schumacher, M. Grun and K. K. Unger, *Microporous Mesoporous Mater.*, 1999, **27**, 201.
51 M. Kruk and M. Jaroniec, *Chem. Mater.*, 2000, **12**, 222.
52 R. Ryoo, I.-S. Park, S. Jun, C. W. Lee, M. Kruk and M. Jaroniec, *J. Am. Chem. Soc.*, 2001, **123**, 1650.
53 L. Chen, T. Horiuchi, T. Mori and K. Maeda, *J. Phys. Chem. B*, 1999, **103**, 1216.
54 W. Zhang, T. R. Pauly and T. J. Pinnavaia, *Chem. Mater.*, 1997, **9**, 2491.
55 Y. D. Glinka, C. P. Jaroniec and M. Jaroniec, *J. Colloid Interface Sci.*, 1998, **201**, 210.